AIP Advances

Study of magnetic switch for surface plasmon-polariton circuits

Cite as: AIP Advances **11**, 045222 (2021); https://doi.org/10.1063/5.0040674
Submitted: 25 December 2020 . Accepted: 05 April 2021 . Published Online: 20 April 2021

Alessandro Bile, Ricardo Pepino, and Eugenio Fazio

Study of magnetic switch for surface plasmon-polariton circuits

Cite as: AIP Advances 11, 045222 (2021); doi: 10.1063/5.0040674
Submitted: 25 December 2020 • Accepted: 5 April 2021 •
Published Online: 20 April 2021

Alessandro Bile,[a] Ricardo Pepino, and Eugenio Fazio

AFFILIATIONS

Department of Fundamental and Applied Sciences for Engineering, Sapienza Università di Roma, 00161 Roma, Italy

[a]Author to whom correspondence should be addressed: alessandro.bile@uniroma1.it

ABSTRACT

In recent years, technological development has focused on the construction of ever smaller devices, characterized by dimensions limited to the nanometer order and by a very low energy requirement to be able to function. This allows them to be integrated into chips, which are then able to perform many tasks from filtering to computation. Here, we present a magnetic switch capable of working with surface plasmon polaritons.

I. INTRODUCTION

Surface Plasmon Polaritons (SPPs) are electromagnetic waves coupled to oscillations of electron plasma propagating at the interface between two materials, characterized by dielectric constants with opposite sign.[1,2] SPPs localize their electromagnetic field inside the surrounding media within volumes smaller than the light diffraction limit: this characteristic behavior makes them very attractive to realize ultracompact nanophotonic chips. This allows the construction of nanophotonic chips, leading to a double advantage: they are able to overcome the speed limitation of electronics and the critical dimensions of photonics.[3] For this reason, in the last period, many plasmonic components and devices have been studied such as waveguides, modulators, and couplers.[4–6] Among the passive devices studied so far, plasmonic waveguide-rings and disk resonators have been theoretically and experimentally proven to have several functionalities such as filtering, wavelength division multiplexing, and coupling.[7–9,13,16] In plasmonic resonators, localized surface plasmon polariton modes show a low-quality factor about several tens, which is not enough to reach a high contrast in the modulation of the plasmons. In contrast, traveling resonant modes in waveguide-ring resonators have a higher quality factor.[7,10,13] A ring resonator consists of a circular optical resonator with a unidirectional coupling mechanism to a straight waveguide. For precise wavelengths, the resonance condition is verified when the waves interfere constructively inside the ring, which introduces a significant phase shift near the resonance and resonantly enhances the interaction. In this work, we present a plasmonic signal switch controlled through the application of an external magnetic field. The switch consists of an SPP guide coupled together with a resonant plasmonic ring surrounded by an additional ferromagnetic dielectric ring. In resonance or anti-resonance conditions, the energy transferred to the resonator varies, consequently modulating the transmission along the waveguide. The resonance is controlled by the magnetization of the ferromagnetic dielectrics, which, being affected by an external field, can go into saturation in the upward or downward direction. Following these different magnetizations, the wavevector of the plasmonic wave propagating in the ring varies, bringing it into resonance or anti-resonance behaviors.

II. STRUCTURE OF THE DEVICE

Plasmonic circuits allow us to overcome the limitations presented by electrical and optical circuits; their usefulness lies in the possibility of controlling and manipulating the plasmonic properties. Recent studies show how the properties of plasmons can be modulated more or less rapidly through temperature,[11,12] voltage,[13,14] and optical signals.[15,16] In all cases, the control mechanism acts either on the absorption or on the wavevector and the choice of one system over another depends on various factors. Among these, we find the switching speed, which defines the dynamic response of the circuit, and the modulation of its intensity is important to

quantify the effect it produces, in order to design an appropriate specific device with simplicity and effective cost. In general, temperature-controlled devices have a switching speed of the millisecond order but are able to present greater modulation. The electronic ones guarantee a fast switching speed and a strong modulation, while the optical ones depend on the particular case. In this work, the SPPs are controlled through an external magnetic field. This has multiple advantages: the magnetic field modifies the optical properties of a material based not only on its direction but also on its intensity[17–19] and also allows for commutation speeds of the order of femtoseconds to be reached.[17] However, the performance of the ultrafast magnetoplasmonic modulators in the visible and near-infrared ranges generally suffers from a small change in the SPP wave number,[20,21] which requires a larger device size of at least tens of micrometers to achieve a good interaction between the external magnetic field and the SPP. It is possible to enhance the wavenumber change, thanks to photonic crystals:[22] the transmission bandwidth is limited by photonic bandgaps. A more compact magnetoplasmonic interferometer using a hybrid ferromagnetic structure was successfully demonstrated to present 2% modulation requiring a waveguide length of 20 μm,[23,24] which can be improved to 12% modulation[25] by adding a dielectric layer with a higher refractive index. In this paper, we propose and study an SPP resonator by using a single-interface waveguide coupled to a ring resonator that is immersed in a ferromagnetic dielectric material. First, without the application of any external factor, we found that the transmission and reflectivity of the structure depend on the geometrical parameters that define the disk-waveguide system. Second, by applying an external magnetic field, there is a variation of the SPP wavevector and, consequently, there is an on/off switching based on the direction of the magnetization. The scheme of the simulated device is shown in Fig. 1 and can be divided into three distinct areas. The first region, where the excitation of the SPP takes place, consists of a silver interface with a length of 1745 μm. It was chosen to use silver as the dielectric metal as it has a minor imaginary component and therefore gives rise to a lower attenuation.

The propagation geometry is shown in Fig. 1. We assumed for simplicity a 2D structure, which is infinite along the z direction. The SPP propagates along the x direction (from left to right in Fig. 1) and is evanescently confined along the y direction. The separation interface between a thin layer of silver[26] about 4 μm long and a bulk of silicon oxide constitutes a waveguide for the SPPs. As will be explained later, dielectric materials have been manually defined neglecting the spectral dependence. The second region is in the center of the propagation and consists of a ring structure formed by three layers: an outer ring of Bismuth Iron Garnet (BIG), a dielectric material with ferromagnetic behavior; a second metal ring of gold;[26] and an inner disk to everything about BIG. The outer ring has an outer radius of 255 nm and an inner radius of 200 nm, while the metal layer ranges from 200 to 150 nm. Gold was chosen because it has a bigger imaginary part than silver. This allows a greater penetration depth and consequently a better coupling to the ring resonator. The third region is identical to the first one and constitutes the output of the structure. The wavelength used is 800 nm. The dispersion relation of the dielectric materials is almost constant around this value. Therefore, when passing to the 3D model, we expect negligible variation of the resonant frequency.[27] Numerically, we have represented silicon oxide with a relative dielectric constant e = 2.25 and a refractive index nd = 1.5; for the BIG, we considered a relative dielectric constant e = 6.25 and a refractive index nf = 2.5.[27–30] The width of the gold ring is low enough to ensure coupling of the SPP on both sides of the ring. The higher refractive index on the inner side allows a lesser penetration of the field inside, achieving a better outcoupling of the SPP from the ring to the single-interface waveguide. On a real device, the structure would look exactly as the one shown in Fig. 1 (looking it from above) and it can be easily produced within the current technology. Indeed, the recently rapid development of nanotechnologies in different application fields has led to the fabrication of circular or rectangular nanodisk cavity resonators.[32,33] The

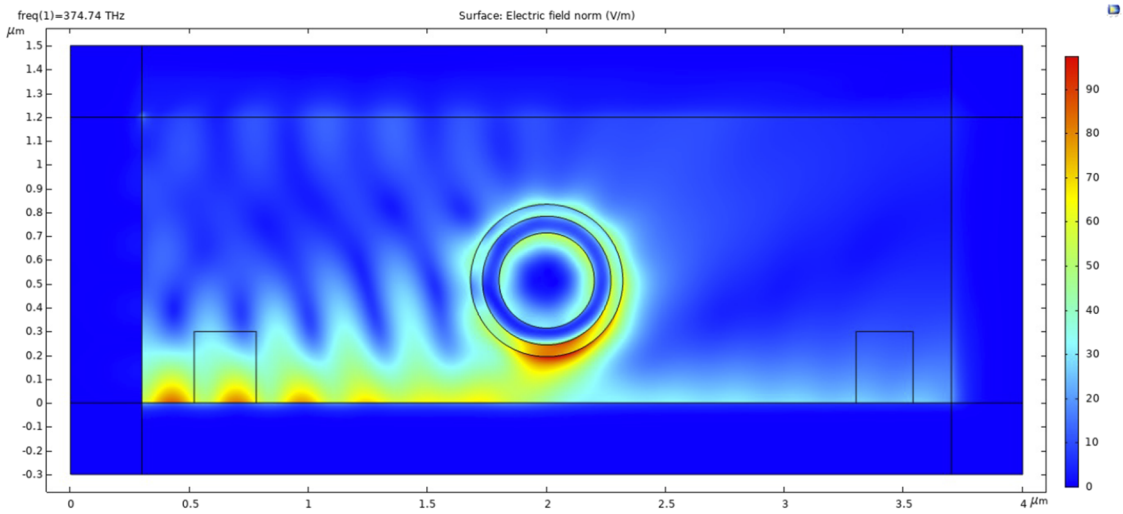

FIG. 1. Schematic representation of the simulated structure with used materials.

generation of the SPP can be achieved by using end-fire techniques or by the use of grooves with suitable periodicity for coupling.[1] The ferromagnetic behavior of the BIG has been schematized following Voigt's theory of the opto-magnetic behavior, according to which the relative dielectric constant is a tensor and can vary as a function of the magnetization of the material according to the relationship[31]

$$\overleftrightarrow{\epsilon_r} = \epsilon_r \begin{bmatrix} 1 & i\beta M_z & -i\beta M_y \\ -i\beta M_z & 1 & i\beta M_x \\ i\beta M_y & -i\beta M_x & 1 \end{bmatrix}, \quad (1)$$

where M represents the magnetization of the material, β describes the opto-magnetic susceptibility, and their product gives the magneto-optical constant of the material. For the BIG, considering a wavelength of 800 nm, $|\beta M| \cong 0.06$[27–30] in the magnetization saturation regime. The trilayer thus obtained represents an IMI (insulator/metal/insulator) ring guide coupled with the rectilinear metal guide below. The effectiveness of the coupling, and therefore the modulation of the SPP, depends on the distance between the straight guide and the ring.

III. RESONANT CONDITION

The optical distance traveled by the SPP inside the disk is equal to

$$L_d = 2\pi r N_{eff}, \quad (2)$$

where n_{eff} indicates the effective refractive index of the resonator ring. In order to obtain resonance, the following condition must be verified:

$$L_d = m\lambda_{sp}, \quad (3)$$

which corresponds to requiring an optical distance equal to a multiple of the wavelength in the order of the SPP in order to obtain constructive interference. As can been seen, the resonance depends on the radius of the ring and on its effective refractive index. The latter, in turn, depends on the thickness of the gold ring, on the thickness of the outer BIG, and on the direction of the magnetization. Thus, we can write

$$L_d(r, M) = 2\pi N_{eff}(r, M) r. \quad (4)$$

IV. RESULTS AND DISCUSSION

From the above considerations, the propagation and resonance properties of the circular structure were analyzed by varying the radius of the inner ring, the thickness of the gold ring, the thickness of the outer dielectric ferromagnetic ring, and the distance of the ring from the interface. Furthermore, the optimization process envisaged three different situations: absence of magnetization $M_z = 0$ and magnetization in the positive z direction $+M_z \neq 0$ or in the negative z direction $-M_z \neq 0$. When the plasmon-polariton wave reaches the ring, it couples with both the metal interface and the ferromagnetic dielectric interface (Fig. 2), which, however, immediately loses efficiency in favor of both radiative losses and the metal interface.

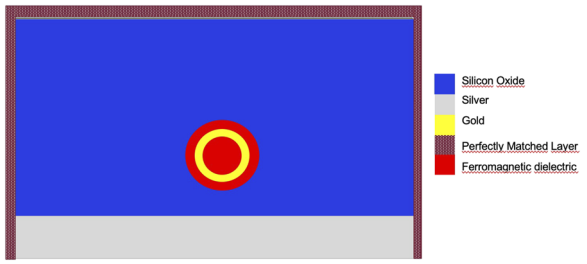

FIG. 2. Schematic representation of the simulated structure with used materials.

As we will see, the coupling of the two structures (linear and ring guides) is strictly dependent on the resonance of the ring: in the resonance regime, a lot of radiation is transferred to the ring, canceling the subsequent rectilinear propagation; instead, in the anti-resonance regime, little or no transfer takes place and the rectilinear propagation remains fed.

By varying the internal radius of the BIG ring and the thickness of the gold one, an oscillating modulation of the average intensity of the SPP wave is observed in the annular structure (Fig. 3) and in the output plasmon guide (Fig. 4), both in the absence of magnetization. Comparing Fig. 3 with Fig. 4, we note that the two have a complementary trend: when the ring enters into resonance, the light is coupled effectively and there is a lower output power; similarly, when the ring exits the resonance, the coupling efficiency decreases

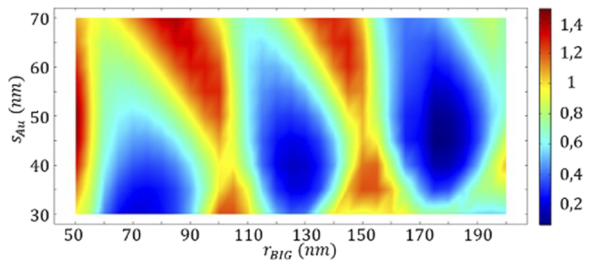

FIG. 3. Trend of the average power inside the ring as the radius of the inner ring varies from 50 to 200 nm and the radius of the golden ring varies from 30 to 70 nm both with a step of 10 nm.

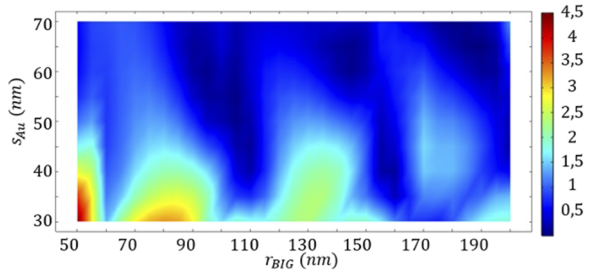

FIG. 4. Trend of the maximum output power as the radius of the inner ring varies from 50 to 200 nm and the radius of the golden ring varies from 30 to 70 nm both with a step of 10 nm.

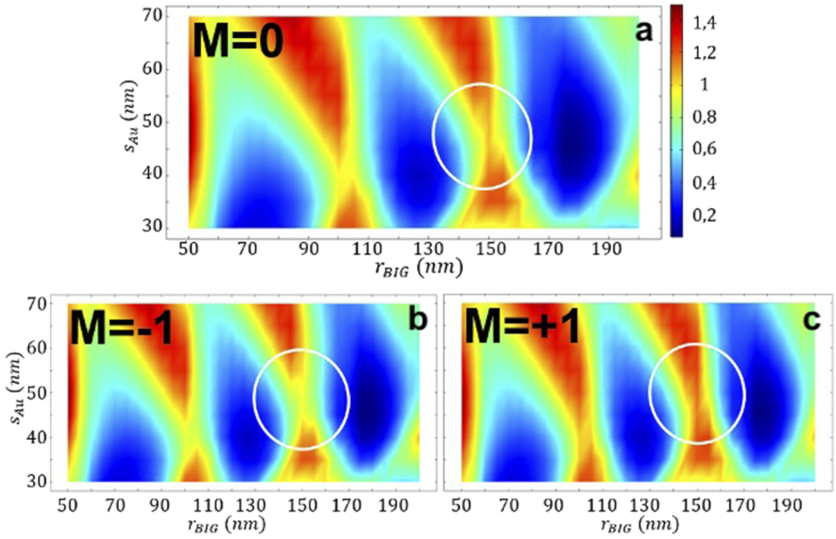

FIG. 5. Trend of the average intensity inside the disk power as the radius of the inner ring varies from 50 to 200 nm and the radius of the golden ring varies from 30 to 70 nm both with a step of 10 nm in the case of (a) absence magnetization m = 0, (b) magnetization m_-, and (c) magnetization m_+.

with a consequent increase in the output intensity. By decreasing the radii of the annular structures, a decrease in the intensity transported is observed due to both an increase in radiative losses by the annular structure and an incomplete decoupling of the SPP from the ring resonator. This means that the SPP propagating on the ring will be much more dampened (having only traveling modes). Therefore, the power coupling to the single interface will be much lower, which means a lower transmission instance than in the previous cases and regardless of the resonance. For this reason, to have a better quality factor, it is suggested to have a structure as close as possible to the resonance mode [$L_d = l_{sp}$ in Eq. (3)]. The resonant behavior of the ring can now be modulated with active magnetization of the BIG, as shown in Fig. 5: the white circles in Fig. 5 show the different states of resonance as a function of the magnetization of the BIG.

The coupling of the plasmon with the ring turns out to be more effective in the m_+ case than in the m_- case. Within the ranges studied, 50–200 nm for the radius of the inner ring and 30–70 nm for the gold thickness (varied with a step of 5 nm), the sharper contrast of higher power was recognized for the values 145 and 50 nm. In this case, they are obtained as $P_{m_-} = 1.14\ \frac{W}{m^2}$ and $P_{m_+} = 0.78\ \frac{W}{m^2}$. Following these results, we therefore focused on a narrower range (1 nm step), a radius range between 140 and 150 nm and gold thickness between 45 and 55 nm. In this way, we have further increased the contrast to $\Delta P = 0.37\ \frac{W}{m^2}$. Considering the dependence of the structure on the height of the resonant ring with respect to the interface, in the case of the absence of magnetization, an increase in the maximum input power can be seen in parallel with the increase in the height value. In Fig. 6, we report the trends of the average power inside the resonant ring. It is important to note that the coupling efficiency has an increasing trend up to 270 nm; exceeding this value, the interaction decreases since the plasmon "feels" less the presence of the ring. The most direct consequence is a linear increase in the maximum transmitted power, as shown in Figs. 6(c) and 6(a),which shows the reduction of its reflectivity.

Repeating the study with magnetization, the coupling between the plasmon and the resonant ring is more effective in the m_+ case.

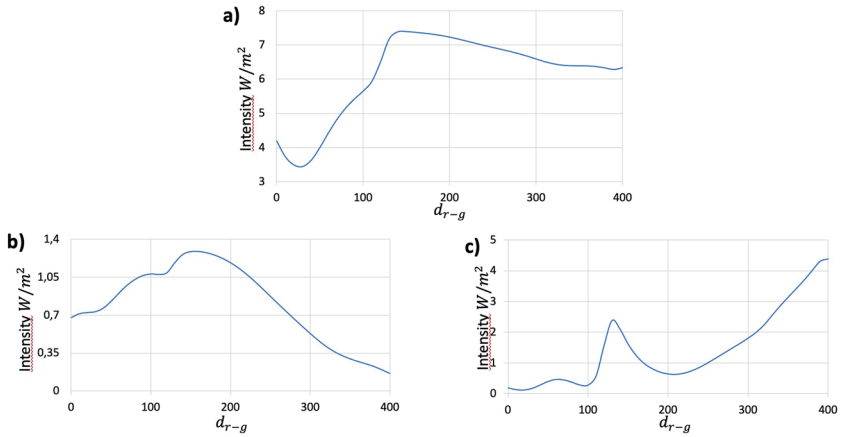

FIG. 6. Trend (a) of the maximum input power, (b) of the average power inside the ring, and (c) of the maximum output power as the ring height varies from 103 to 503 nm with a step of 10 nm.

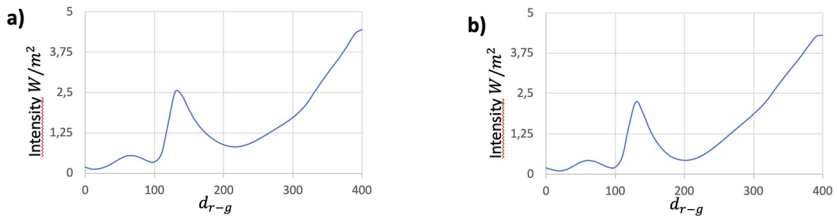

FIG. 7. Trend of the maximum output power as the height of the resonant ring varies from 103 to 503 nm with a step of 10 nm in the case of (a) m_- and (b) m_+.

A higher maximum output power can be noticed in the m_- case, as shown in Fig. 7, which shows the trend of the maximum power in the m_- and m_+ cases. The greatest contrast between the two configurations is achieved when a height of 264 nm is reached.

The maximum contrast was found at the height value of 264 nm, for which the following power values were recorded, $P_{m_-} = 1.56\ \frac{\mathrm{W}}{\mathrm{m}^2}$ and $P_{m_+} = 0.96\ \frac{\mathrm{W}}{\mathrm{m}^2}$, and the following contrast index was recorded, $\Delta P = 0.60\ \frac{\mathrm{W}}{\mathrm{m}^2}$. Finally, the device we are presenting has been investigated by varying the thickness of the external dielectric ferromagnetic ring in two different configurations. Once the center of the height of the resonant ring was kept constant with respect to the waveguide, a second time, the lowest point of the resonant ring was kept constant.

In the first case, by maintaining constant the height of the center of the resonant ring, when the thickness of the layer relative to the external ferromagnetic dielectric increases, an increase in the radius of curvature of the structure is also observed. This results in a dependence of the effective refractive index of the SPP, which propagates on the silver waveguide as a function of the position below the resonant ring and of the effective refractive index of the ring resonator as a function of the thickness of the external BIG. In this case, the SPP propagating on the single interface, once it gets under the ring resonator, enters inside a MIM (Metal/Insulator/Metal) waveguide, whose width decreases until it gets under the center of the ring. This means that the SPP gets compressed more and more while propagating, resulting in an increase in its effective refractive index. Therefore, increasing the width of the BIG ring will cause an increase in SPP compression. In summary, there will be an increase in the refractive index, followed by a change in the reflectivity of the structure. This can be seen from Fig. 8(a), which shows that the input intensity has an oscillating behavior with increasing thickness.

The variation of the mode present in the IMI guide is also observed, which determines a change in the coupling. Indeed, looking at Eq. (3), it is clear that the resonance depends on the effective refractive index that the SPP of the IMI guide sees. Changing the width of the outer BIG also influences the refractive index because the intensity of the SPP will feel less the outer silicon dioxide. This will induce, as shown in Fig. 8(b), an oscillating behavior of the average intensity inside the resonant structure as a function of the width of the BIG ring.

It is interesting to observe the maximum intensity between the two peaks: as the thickness increases, we notice worsening of the coupling; in fact, the smaller the thickness, the greater the quantity of SPPs that manage to couple. Figures 9(a) and 9(b) show how the trend of the average power inside the resonant structure and the trend of the output power are complementary. In fact, with each decrease in the maximum output power, there is a corresponding increase in the average power inside the resonant ring and vice versa.

Considering a non-zero magnetization of the m_- type, a less efficient coupling between the plasmon and the resonant structure is observed for thicknesses less than 70 nm. After that, the behavior becomes opposite even if characterized by a lower intensity. For thicknesses greater than 70 nm, the maximum output power will be in the case of m_+. From Fig. 11(a) and in Fig. 11(b), it can be seen that the highest power contrast corresponds to a thickness of 36 nm. By making a zooming analysis within the range 24–48 nm in steps

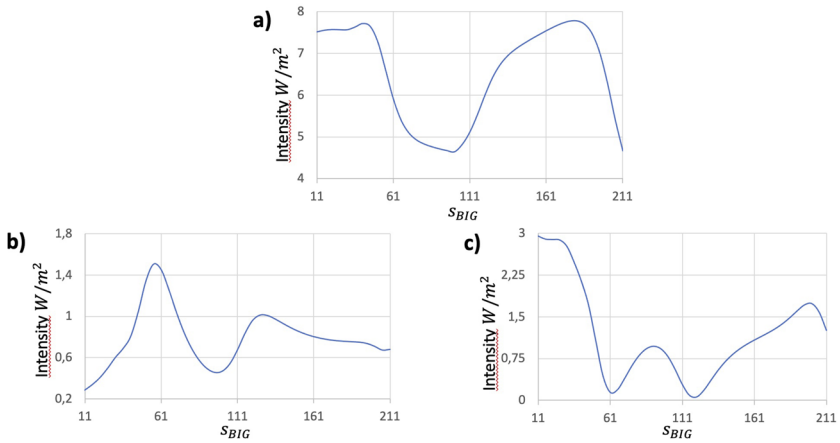

FIG. 8. Trend (a) of the maximum input power, (b) of the average power within the resonant structure, and (c) of the maximum output power as the thickness of the ferromagnetic ring varies from 11 to 211 nm with a step of 5 nm.

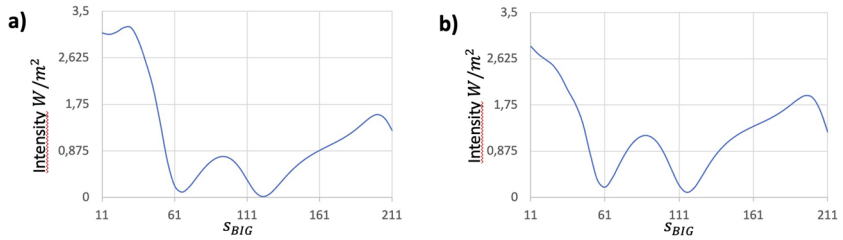

FIG. 9. Trend of the maximum output power as the thickness of the ferromagnetic ring varies from 11 to 211 nm with a step of 5 nm in the case of (a) m_- and (b) m_+.

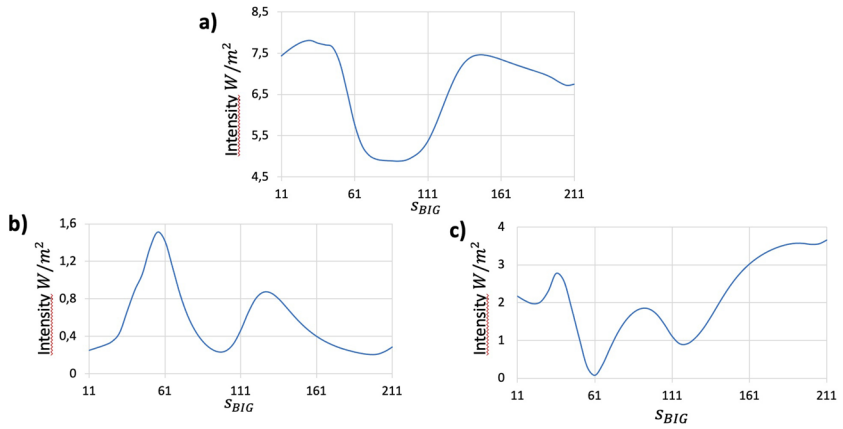

FIG. 10. (a) Trend of the maximum input power, (b) of the average power inside the resonant structure, and (c) of the maximum output power as the thickness of the ferromagnetic ring varies from 11 to 211 nm with a step of 5 nm.

of 1 nm, it is observed that the maximum of the effective contrast corresponds to a height equal to 34 nm, for which power values are equal to $P_{m_-} = 3.07\ \frac{\mathrm{W}}{\mathrm{m}^2}$ and $P_{m_+} = 2.14\ \frac{\mathrm{W}}{\mathrm{m}^2}$.

By keeping the lowest point of the resonant structure constant, a gradual increase in the effective refractive index is observed as the lowest point is approached. In this case, contrary to the preceding one, the effective refractive index decreases while increasing the BIG ring width. This is due to the fact that the resonant structure increases its height from the single interface below, decompressing the SPP. Nevertheless, as can be seen from Fig. 11(a), the reflectivity of the structure has the same trend as in the other case. Hence, reflectivity does not depend on the actual change in refractive index seen by the SPP when switching from a single to a dual interface. It depends on the continuous change in its value under the resonant structure that denotes the presence of some cavity effect. The average power inside the structure has a trend similar to that of the previous case. For the output intensity, since the height of the gold ring increases, the SPP will feel less its presence. The most direct consequence is a linear increase in the maximum transmitted power, as can be seen in Fig. 10(c).

We report the results derived from the ignition of the field in Fig. 11(a) by magnetization m_- and in Fig. 11(b) by magnetization m_+. The maximum contrast found is for a thickness equal to 134 nm, to which the following values correspond: $P_{m_-} = 1.11\ \frac{\mathrm{W}}{\mathrm{m}^2}$ and $P_{m_+} = 1.94\ \frac{\mathrm{W}}{\mathrm{m}^2}$.

V. CONCLUSIONS

The analyses conducted so far show how the magnetoplasmon switch is based on the interaction between the propagation modes of a single-interface plasmon guide and those of an asymmetric ring IMI resonator, always plasmonic, within a magnetizable structure. The interaction between the guide and the resonator depends on the resonance of the structure: in the resonance case, there is a strong transfer of energy from the single-interface guide to the resonator

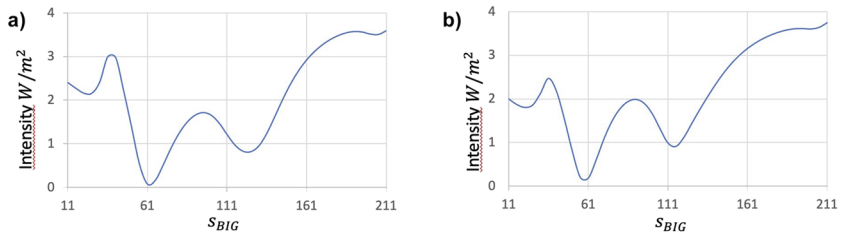

FIG. 11. Trend of the maximum output power as the thickness of the ferromagnetic ring varies from 126 to 141 nm with a step of 1 nm in the case of (a) m_- and (b) m_+.

TABLE I. Optimized parameters of the magnetoplasmonic switch.

Height of the center of the resonator	264 nm
Thickness of the gold ring	53 nm
External dielectric ferromagnetic thickness	134 nm
Inner ring radius	147 nm

and therefore a low transmissivity, while in the absence of resonance, there is less energy transfer and consequently greater output power. The efficiency of the guide-resonator interaction varies according to the geometric parameters of the structure and the direction of magnetization. In fact, since the resonator has a circular shape, in order to get the resonance, the optical path inside it must necessarily be a multiple of the wavelength of the SPP. This, in turn, depends on the effective refractive index and the geometric parameters of the structure. The application of a magnetic field changes the dispersion relationship of the SPPs in a non-reciprocal manner. From this, it follows that $k_x(m_+) \neq k_x(m_-)$; therefore, based on the direction of the external magnetic field applied, it is possible to vary the optical path inside the ring and ultimately modify the interaction efficiency between the guide and the resonator. We obtained the optimal values of the geometric parameters corresponding to the maximum power contrast, which are shown in Table I. In this way, it was possible to switch from a contrast of $\Delta P_{m_+} = 0.08\ \frac{W}{m^2}$ to $\Delta P_{m_+} = 0.83\ \frac{W}{m^2}$, i.e., obtaining an increase by a factor of 10.

We are currently working on improving the output contrast even more. This depends on the optical path seen by the plasmon inside the IMI guide and therefore on the geometric parameters of the structure and on the wavevector of the SPP. This can be controlled through the application of an external magnetic field. If we consider

$$\Delta k_x = -k^0{}_x \frac{\epsilon_{xz,2}}{\sqrt{\epsilon_1 \epsilon_2}(1 - \epsilon^2{}_2/\epsilon^2{}_1)} + O(\epsilon^2{}_{xz}), \tag{5}$$

we see that the maximum obtainable value is equal to $2\Delta k_x$. The uses of a structure with the characteristics of the magnetoplastic switch that we have presented are many. It can be used as a filter, exploiting the strong sensitivity of the structure to the wavelength; furthermore, the application of the external magnetic field allows us to shift the resonance: this means to change both the frequency of the filter and its sensitivity. Furthermore, in a world in which artificial intelligence is becoming more important, devices capable of saving the memory of many states are becoming fundamental. Our magnetoplasmonic structure can exploit the magnetization to switch the output and to project itself toward one of the two possible states. Moreover, it is possible to obtain a permanent memory effect thinking of working with ferromagnetic materials with a coercive field other than zero.

AUTHOR'S CONTRIBUTIONS

All authors contributed equally to this work.

DATA AVAILABILITY

The data that support the findings of this study are available from the corresponding author upon reasonable request.

REFERENCES

[1] S. A. Maier, *Plasmonics: Fundamentals and Applications* (Springer, Berlin, 2007).
[2] H. Raether, *Surface Plasmons* (Springer, Berlin, 1986).
[3] E. Ozbay, "Plasmonics: Merging photonics and electronics at nanoscale dimensions," Science **311**, 189–193 (2015).
[4] A. V. Zayats, I. I. Smolyaninov, and A. A. Maradudin, "Nano-optics of surface polarities," Phys. Rep. **408**, 131–314 (2005).
[5] T. W. Ebbesen, C. Genet, and S. I. Bozhevolnyi, "Surface-plasmon circuitry," Phys. Today **61**(5), 44–50 (2008).
[6] D. K. Gramotnev and S. I. Bozhevolnyi, "Plasmonics beyond the diffraction limit," Nat. Photonics **4**, 83–94 (2010).
[7] I. Chremmos, O. Schwalb, and N. Uzunoglu, *Photonic Microresonator Research and Applications* (Springer, Boston, 2010).
[8] C. Manolatou, M. J. Khan, S. Fan, P. R. Villeneuve, and H. A. Haus, "Coupling of modes analysis of resonant channel add-drop filters," IEEE J. Quantum Electron. **35**(9), 1322–1331 (1999).
[9] A. Yariv, "Universal relations for coupling of optical power between microresonators and dielectric waveguides," Electron. Lett. **36**, 321–322 (2000).
[10] J. Pae, S. Im, K. Ho, C. Ri, S. Ro, and J. Herrmann, "Ultracompact high-contrast magneto-optical disk resonator side-coupled to a plasmon waveguide and switchable by and external magnetic field," Phys. Rev. B **98**, 041406 (2018).
[11] T. Nikolajsen and K. Leosson, "Surface plasmon polariton based modulators and switches operating at telecom wavelengths," Appl. Phys. Lett. **85**, 5833–5835 (2004).
[12] J. Gosciniak, S. I. Bozhevolnyi, T. B. Andersen, V. S. Volkov, J. Kjelstrup-Hansen, L. Markey, and A. Dereux, "Thermo-optic control of dielectric-loaded plasmonic waveguide components," Opt. Express **18**, 1207–1216 (2010).
[13] S. Randhawa, S. Lacheze, J. Renger, A. Bouhelier, R. E. de Lamaestre, A. Dereux, and R. Quidant, "Performance of electro-optical plasmonic ring resonators at telecom wavelengths," Opt. Express **20**(8), 2354–2362 (2012).
[14] A. Agrawal, C. Susut, G. Stafford, U. Bertocci, B. McMorran, H. J. Lezec, and A. A. Talin, "An integrated electrochromic nanoplasmonic optical switch," Nano Lett. **11**, 2774–2778 (2011).
[15] K. F. MacDonald, Z. L. Sámson, M. I. Stockman, and N. I. Zheludev, "Ultrafast active plasmonics," Nat. Photonics **3**, 55–58 (2009).
[16] M. P. Nielsen and A. Elezzabi, "Ultrafast all-optical modulation in a silicon nanoplasmonic resonator," Opt. Express **21**(12), 20274–20279 (2013).
[17] R. F. Wallis, J. J. Brion, E. Burstein, and A. Hartstein, "Theory of surface polaritons in anisotropic dielectric media with application to surface magnetoplasmons in semiconductors," Phys. Rev. B **9**(8), 3424–3437 (1974).
[18] G. Armelles, A. Cebollada, A. García-Martín, and M. U. González, "Magnetoplasmonics: Combining magnetic and plasmonic functionalities," Adv. Opt. Matter **1**, 10–35 (2013).
[19] N. Maccaferri, I. Zubritskaya, I. Razdolski, I. A. Chioar, V. Belotelov, V. Kapaklis, P. M. Oppeneer, and A. Dmitriev, "Nanoscale magnetophotonics," J. Appl. Phys. **127**, 080903 (2020).
[20] B. Selpuveda, L. M. Lechuga, and G. Armelles, "Magnetooptic effects in surface plasmon polaritons slab waveguides," J. Lightwave Technol. **42**(2), 945–955 (2006).
[21] J. B. Khurgin, "Optical isolating action in surface plasmon polaritons," Appl. Phys. Lett. **89**, 251115 (2006).
[22] Z. Yu, G. Veronis, Z. Wang, and S. Fan, "One-way electromagnetic formed at the interface between a plasmonic metal under a static magnetic field and a photonic crystal," Phys. Rev. Lett. **100**, 023902 (2008).
[23] V. V. Temnov, G. Armelles, U. Woggon, D. Guzatov, A. Cebollada, A. Garcia-Martin, J.-M. Garcia-Martin, T. Thomay, A. Leitenstorfer, and R. Bratschitsch, "Active magneto-plasmonics in hybrid metal–ferromagnet structures," Nat. Photonics **4**, 107–111 (2010).
[24] D. Martin-Becerra, V. V. Temnov, T. Thomay, A. Leitenstorfer, R. Bratschitsch, G. Armelles, A. Garcia-Martin, and M. U. Gonzalez, "Spectral dependence of the magnetic modulation of surface plasmon polaritons in noble/ferromagnetic/noble metal films," Phys. Rev. B **86**, 035118 (2012).

[25]D. Martin-Becerra, J. B. Gonzalez-Diaz, V. V. Temnov, A. Cebollada, G. Armelles, T. Thomay, A. Leitenstorfer, R. Bratschitsch, M. A. Garcia, and M. U. Gonzalez, "Enhancement of the magnetic modulation of surface plasmon polaritons in Au/Co/Au films," Appl. Phys. Lett. **97**, 183114 (2010).
[26]P. B. Johnson and R. W. Christy, "Optical constants of the noble metals," Phys. Rev. B **6**(12), 4370–4379 (1972).
[27]S. Yao, T. Sato, K. Kaneko, S. Murai, K. Fujita, and K. Tanaka, "Faraday effect of bismuth iron garnet thin film prepared by mist CVD method," Jpn. J. Appl. Phys., Part 1 **54**, 063001 (2015).
[28]K. S. Ho, S. J. Im, J. S. Pae, C. S. Ri, Y. H. Han, and J. Herrmann, "MSwitchable plasmonic routers controlled by external magnetic fields by using magneto-plasmonic waveguides," Nature **8**(8), 10584 (2018).
[29]A. Davoyan and N. Engheta, "Electrically controlled one-way photon flow in plasmonic nanostructures," Nat. Commun. **5**, 5250 (2014).
[30]A. Dutta, A. V. Kildishev, V. M. Shalaev, A. Boltasseva, and E. E. Marinero, "Surface plasmon opto-magnetic field enhancement for all-optical magnetization switching," Opt. Mater. Express **7**(12), 4316–4327 (2017).
[31]A. K. Zvezdin and V. A. Kotov, *Modern Magnetooptics and Magnetooptical Materials* (IOP Publishing, Bristol, UK, 1997).
[32]F. Hao, P. Nordlander, M. T. Burnett, and S. A. Maier, "Enhanced tunability and linewidth sharpening of plasmon resonances in hybridized metallic ring/disk nanocavities," Phys. Rev. B **76**, 245417 (2007).
[33]A. Moreau, C. Ciracì, J. J. Mock, R. T. Hill, Q. Wang, B. J. Wiley, A. Chilkoti, and D. R. Smith, "Controlled-reflectance surfaces with film-coupled colloidal nanoantennas," Nature **492**, 86–89 (2012).